RSC Advances

ARTICLE

Growth and Humidity-Dependent Electrical Properties of Bulk-like MoS_2 Thin Films on Si

Received 00th January 2015,
Accepted 00th January 2015

DOI: 10.1039/x0xx00000x

www.rsc.org/

Y. J. Liu,[a] L. Z. Hao,[a] W. Gao,[a] Y. M. Liu,[a] G. X. Li,[a] Q. Z. Xue,[a] W. Y. Guo,[a] L. Q. Yu,[a] Z. P. Wu,[b] X. H. Liu,[b] H. Z. Zeng[b] and J. Zhu[b]

Bulk-like molybdenum disulfide (MoS_2) thin films were deposited on Si substrates using dc magnetron sputtering technique and *n*-MoS_2/*p*-Si junctions were fabricated at room temperature (RT) and 400 °C, respectively. The typical oscillating modes of E^1_{2g} and A_{1g} were shown in the Raman spectra of the as-grown MoS_2 films. Atomic force microscopy illustrated that the surfaces of the films were composed of dense nanoscale grains and scanning electron microscopy revealed the existence of large quantities of pores in the surface. The current-voltage curves of the junctions showed obvious rectifying characteristics due to the energy-band bending near the interface of MoS_2/Si. The fabricated junctions exhibited humidity-dependent electrical properties. Compared with the one with the MoS_2 film deposited at RT, the junction fabricated at 400 °C showed much more obvious sensing properties to humidity gas. Especially, the sensitivity of the device could be tuned by external electrical fields. In the forward voltage range, the currents increased significantly after the junction was exposed to humidity conditions. The response increased with increasing voltage and reached the saturated value after V=1.9 V. The sensing performance was featured by a high sensitivity, fast response and recovery. The junction current in reverse voltage range decreased under the humidity condition. This was contrary to that in forward voltage range. We also studied the dependence of the sensing response on humidity levels. An almost linear correlation was obtained in the measured range of humidity levels. The sensing mechanisms of the MoS_2/Si heterojunction were proposed.

I Introduction

Due to its good electrical, mechanical and optical properties, molybdenum disulfide (MoS_2) has been studied widely in recent years.[1] MoS_2 has become one of excellent candidates to develop high-performance and multifunctional electronic devices, such as transistors, sensors, and solar cells.[2-4] As one kind of focused electronic materials, the dependence of its electrical properties on the surrounding conditions has drawn considerable attention. Recently, many researchers have focused on the effect of atmosphere humidity on the electrical characteristics of nano materials such as MoS_2 nanoflake, graphene, carbon films, and polymer.[5-8] The studied results show that humidity gas can increase or decrease the electrical resistance of nanoscale materials monotonically. MoS_2-based nanoscale materials are a kind of versatile materials applied in various fields. Thus, it is important to understand the humidity dependence of their electrical properties, not only due to its potential applications in developing new-type humidity sensors, but also due to the fact that large parts of the applications of the electronic device have to face the atmosphere circumstance where humidity influence has to be taken into account. The previous studies about MoS_2-based systems are mostly focused on top- or bottom-gated field-effect transistor devices.[9] In this kind of MoS_2-based sensor device, the electrical properties are dominated by the in-plane conduction mechanisms and the sensing characteristics originate mainly from the single MoS_2 materials. However, few *p-n* junction devices composed of MoS_2 and conventional semiconductors (such as Si) have been reported.[10] As a basic element in various kinds of electronic devices semiconductor *p-n* junctions have been widely used. Compared with single MoS_2 material, MoS_2/Si *p-n* junctions have two advantages. Firstly, the excellent properties of MoS_2, such as gas sensing and photoelectrical properties, could be integrated onto Si semiconductors and the fabrication of multifunctional devices would be realized.[11] Secondly, novel electrical characteristics can be caused by the incorporation of the junction area near the interface.[12]

Based on the above analysis, MoS_2 thin films were grown on *p*-type Si substrates using magnetron sputtering technique and the *n*-MoS_2/*p*-Si heterojunctions were fabricated in this study. The electrical characteristics of the fabricated junctions were investigated. We found that the currents changed largely when the MoS_2/Si junctions were exposed to humidity gas at room temperature (RT) and obvious sensing properties to humidity gas were observed. Especially, the sensing behaviours could be tuned by external electrical fields.

II Experimental section

[a] College of Science, China University of Petroleum, Qingdao, Shandong 266580, People's Republic of China. E-mail: haolanzhong@upc.edu.cn; xueqz@upc.edu.cn
[b] State Key Laboratory of Electronic Thin Films and Integrated Devices, University of Electronic Science and Technology of China, Chengdu 610054, People's Republic of China.

MoS_2 thin films were deposited on (100)-oriented Si substrates using dc magnetron sputtering technique. The MoS_2 powder (purity, 99.9%) were cold-pressed into the sputtered target. The substrates used in this work were *p*-type Si (1.2-1.8 Ω cm). Before the deposition, the substrates were ultrasonically cleaned in sequence by using alcohol, acetone, and de-ionized water. Then, the substrates were dipped into HF solution (~4.0%) for 3 min to remove the amorphous SiO_2 layer from the silicon surface. Subsequently, the Si substrates were immediately moved into the vacuum chamber. Then, the MoS_2 thin films were deposited at RT and 400.0 °C, respectively. During the deposition, the working pressure of argon gas was kept at 1.0 Pa and the sputtering power was about 120.0 W. The film thickness of the as-prepared MoS_2 thin film was about 88.1 nm. After the deposition, indium (In) ohmic electrodes were pressed on MoS_2 thin films and Si, respectively. The schematic illustration of the heterojunction is shown in Fig. 1(a). The MoS_2 films were also grown on insulating Si substrates and the in-plane *I-V* curves were measured to show the humidity sensing properties of single MoS_2 films, the schematic illustration of the device based on a single MoS_2 film is shown in Fig. 1(b).

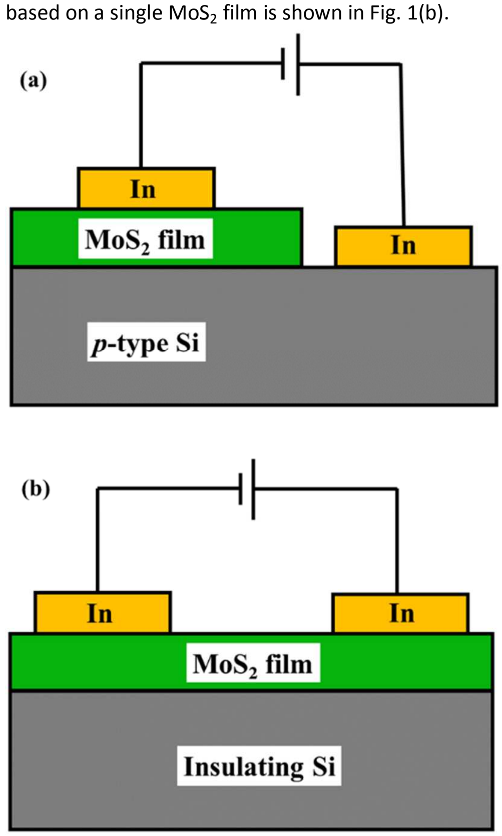

Fig. 1 Schematic illustration of the electrical measurement of (a) MoS_2/Si heterojunction and (b) the device based on a single MoS_2 film.

Samples were characterized using Raman spectroscopy (Renishaw, 514 nm laser). The surface was characterized by atomic forced microscope (AFM, SPM-300HV, SEIKO) and scanning electron microscope (SEM, JSM-7001F, JEOL). The capacitance-voltage (*C-V*) curves were measured using HP4284 source meter. The current-voltage (*I-V*) curves were measured using Keithley2400 source meter at RT. Sensing properties were measured in a chamber by exposing the MoS_2/Si heterojunction to different humidity levels at RT (~300 K).

III Results and discussion

Fig. 2 (a) shows the Raman spectra of the MoS_2 films on Si substrates deposited at RT and 400 °C, respectively. From the figure, we can see that both the films exhibit two characteristic MoS_2 Raman peaks, the E^1_{2g} mode at ~377 cm^{-1} and the A_{1g} mode at ~403 cm^{-1}. The separation between Raman peaks of the film, Δλ= 26 cm^{-1}, is much larger than those for the reported monolayer and several-layer MoS_2.[13] Compared to the film deposited at RT, the MoS_2 film deposited 400 °C shows stronger intensity of the Raman peak. This can be attributed to the improved crystallization quality of the film deposited at a higher temperature. The position of Raman peaks of the films is accord with that of the MoS_2 target used in this work, as shown in Fig. 2(b). This means that the as-deposited films is bulk-like. The E^1_{2g} mode corresponds to the S and Mo atoms oscillating in antiphase parallel to the crystal plane and the A_{1g} mode corresponds to the S atoms oscillating in antiphase out-of-plane, as shown in the insets. These results are consistent with other reported results.[14]

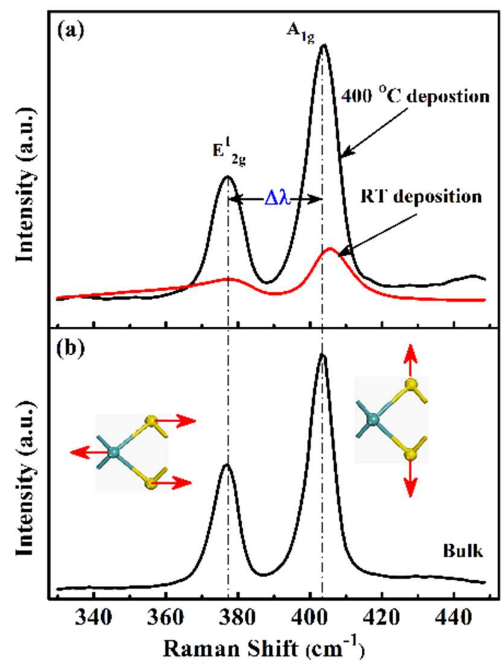

Fig. 2 (a) Raman spectra of the MoS_2 films deposited on Si substrates at RT and 400 °C, respectively. (b) Raman spectrum of the MoS_2 target used in this work. The insets shows the schematic illustration the oscillating mode of E^1_{2g} and A_{1g}.

Fig. 3 (a) shows AFM topographic image of the MoS_2 thin film on Si deposited at RT. From the figure, we can see that the surface of the film is composed of some cone-like grains. The root-mean-square roughness (RMS) of the film is about 1.2 nm, and the average size of grains is about 67.9 nm in diameter. When the deposition temperature increases to 400 °C, the size of the surface grains increases obviously, as shown in Fig. 3(b). According to the measurements, the average size of grains increases 95.9 nm in diameter and the covering ratio of the grains reaches about 89.7%.

The dense nano-level grains could increase the surface-to-volume ratio of the MoS_2 films and this could cause the adsorption of ambient gas molecules on the surface.

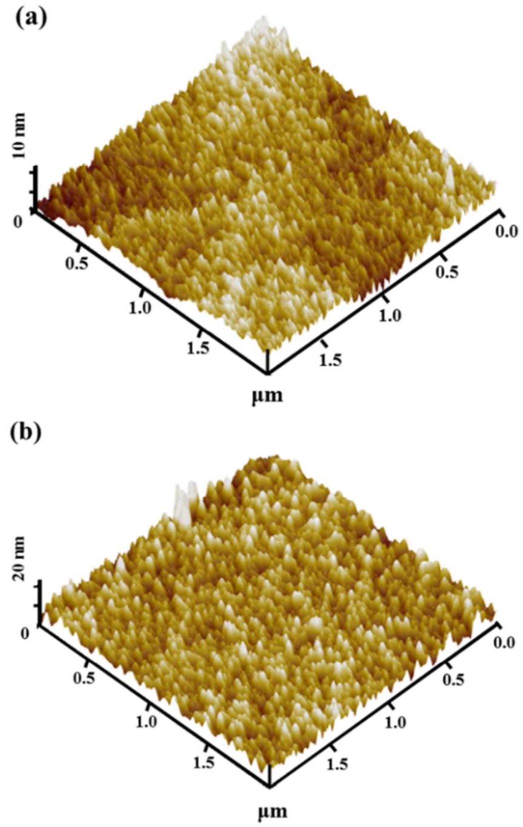

Fig. 3 AFM surface morphology of the MoS_2 thin film deposited on Si at (a) RT and (b) 400 °C, respectively.

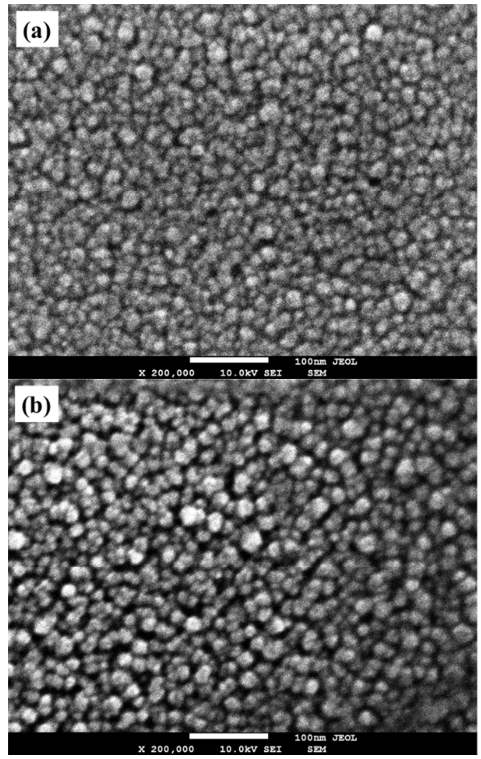

Fig. 4 SEM micrographs of the surface morphology of the MoS_2 films deposited on Si substrates at (a) RT and (b) 400 °C.

Fig. 4(a) shows the SEM micrographs of the surface of the as-grown MoS_2 film deposited at RT. From the figure, large quantities of grain boundaries can be seen obviously and a porous surface is formed. Fig. 4(b) shows the SEM micrographs of the surface of the MoS_2 film deposited at 400 °C. From the figures, we can see that the pore size increase largely when the deposition temperature increases from RT to 400 °C. These grain boundaries could supply effective routes for the absorbed gas molecules to diffuse into the film and even reach the interface area of MoS_2/Si.

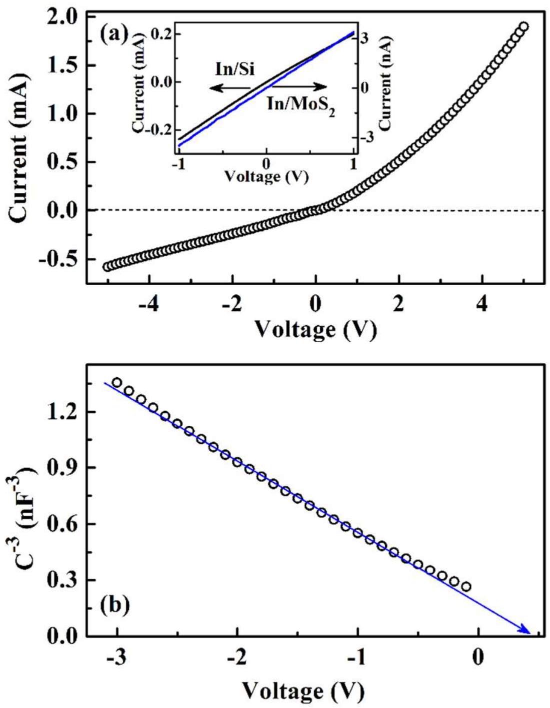

Fig. 5 (a) *I-V* curves of the MoS_2/Si heterojunction fabricated at 400 °C. The inset shows the *I-V* curves of In/MoS_2 and In/Si. (b) Characteristics of C^{-3} vs reverse voltages obtained from *C-V* curve of the fabricated junction.

Fig. 5(a) shows the *I-V* curve of the In/MoS_2/Si/In junction at RT. The MoS_2 film was deposited at 400 °C. From the figure, obvious rectifying behaviour can be seen. The rectifying ratio (I_+/I_-) measured at ±5.0 V is about 3.2. The inset shows the *I-V* curves of the In/Si and In/MoS_2 contacts, respectively. From the figure, almost linear characteristics can be seen. This demonstrates that both the In/MoS_2 and In/Si interfaces belong ohmic contacts. Therefore, the rectifying *I-V* characteristic in the device structure is mainly attributed to the MoS_2/Si junction. The curve of C^{-3} versus reverse voltages obtained from *C-V* curve of the junction is shown in Fig. 5(b). The linear relationship implies that the fabricated heterojunction is graded.[15] According to the intercept on voltage axis, the built-in electrical field (V_{bi}) can be obtained, about 0.42 V.

Fig. 6(a) shows the energy band diagram of isolated MoS_2 and *p*-Si. According to our previous studies, the MoS_2 thin films deposited at 400 °C are *n*-type semiconductors and the energy-band gap (E_{g1}) is about 1.4 eV.[16] For the *p*-Si used in our experiments, the Fermi energy level [E_{F2}=5.0 eV] and energy band gap [E_{g2}=1.12 eV] are taken to construct the band structure and the difference (E_{F2}-E_{V2}) between the Fermi energy level and the top of the valence band is about 0.2 eV.[17] According to $eV_{bi}=E_{F2}-E_{F1}$,[18] the Fermi energy level of the MoS_2 film can be determined, E_{F1}=4.58 eV. This value is in accord with the reported results.[19] When *n*-MoS_2 films are deposited on the surface of *p*-Si, the electrons will flow from MoS_2 into Si at the interface due to the higher Fermi energy level of the MoS_2. The flowing process stops when Fermi levels are equal and the *n*-MoS_2/*p*-Si junction is fabricated, as shown in Fig. 6(b). The built-in electrical field V_{bi} near the interface points from the film to substrate. Due to the formation of the built-in electrical field near the interface, asymmetric characteristics and obvious rectifying effect can be observed from the *I-V* curve in Fig. 5(a).

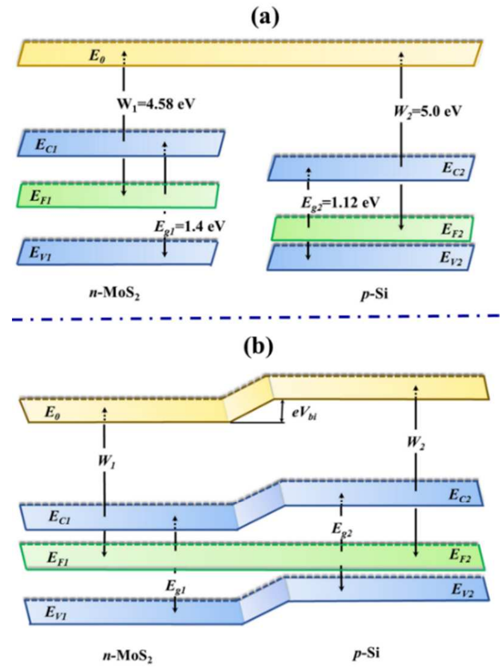

Fig. 6 Schematic illustration of the energy-band structure of MoS_2/Si heterojunctions (a) before and (b) after contact. E_0 is vacuum-energy level, *W* is work function, E_g is energy band gap, E_F is Fermi-energy level, E_C is the bottom of conduction band, and E_V is the top of valence band, respectively.

Fig. 7 (a) shows the *I-V* curves of the *n*-MoS_2/*p*-Si junction in the dry air and humidity conditions of 90%RH, respectively. The MoS_2 film was deposited at 400 °C. The measurements of *I-V* curves were performed 30 min later after the junction were put into the above conditions, respectively. From the figure, we can see that obvious changes of the *I-V* curves of the sample happen when the dry air conditions are changed into 90%RH humidity. As shown in the figure, the forward current increases largely, while the reverse current decreases. This demonstrates that the electrical properties of the junction are dependent on humidity and obvious humidity sensing characteristics are shown. Here, the sensitivity to humidity (*S*) is defined as

$$S = (I_h/I_d - 1) \times 100\% \quad (1)$$

where I_h and I_d represent the current value of the heterojunction in humidity gas and dry air conditions, respectively. At +4.0 V, the current value increases from 1.35 mA to 4.43 mA and the *S* reached ~228.2%. The left inset shows the *I-V* curves of the junction fabricated at RT in dry air and 90% RH, respectively. From the figure, the junction fabricated at RT shows better rectifying characteristics than the junction fabricated at 400 °C and its rectifying ratio is about 17.3. The lower deposition temperature could decrease the element diffusion at the MoS_2/Si interface. Thus, the rectifying properties are enhanced. However, only a little increase of the forward current can be caused when the dry condition is changed into 90%RH and the *S* at +4.0 V is only 27.7%, much smaller than that for the junction fabricated at 400 °C. The right inset shows the *I-V* curves of the single MoS_2 sensor in dry air and 90%RH, respectively. As shown in the figure, the current after the exposure of the device upon humidity condition increases in the whole voltage range. This is complete different with the current change of the junction devices. According to our calculation, the sensitivity of the single MoS_2 sensor is only 48.5% under 90%RH humidity condition.

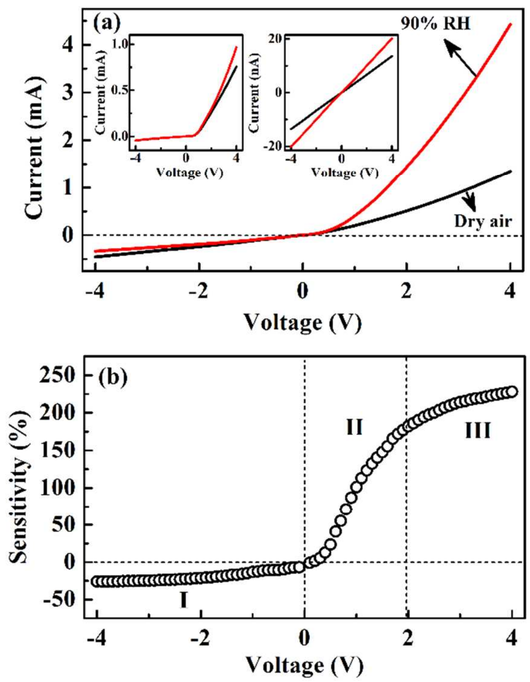

Fig. 7 (a) *I-V* curves of the n-MoS_2/p-Si heterojunction fabricated at 400 °C in dry air and 90% RH, respectively. The insets show the *I-V* curves of the junction fabricated at RT (left) and single MoS_2 films grown on insulating Si at 400 °C (right) in dry air and 90% RH, respectively. (b) Dependence of the sensitivity of the junction to humidity on voltages.

Fig. 7(b) shows the dependence of the sensitivity of the *n*-MoS_2/*p*-Si junction on voltages under the humidity level of 90%RH. From the figure, obvious dependence of the sensitivity on voltages can be seen. This is very different with the sensitivity of single MoS_2 to gas. In the reported single MoS_2-based sensor devices,[20] the sensitivity is independent on external voltage. According our measurements, *S*=23.5% at +0.5 V. With increasing the forward voltage, *S* increases quickly, as shown in the figure. When the voltage increases to +1.9 V, *S* reaches 180.1%. After that, the sensitivity increases slowly and tend to be saturated, as shown in the figure. The dependence of *S* on the reverse voltages is similar with that in the forward voltage range. These sensing characteristics demonstrates that new-type sensor devices with tunable sensing properties can be developed with the *n*-MoS_2/*p*-Si junctions, which is impossible for the single MoS_2-based sensor devices. According to the above analysis, different characteristics of the response to humidity gas in different voltage range must be induced by different sensing mechanisms of the *n*-MoS_2/*p*-Si junction.

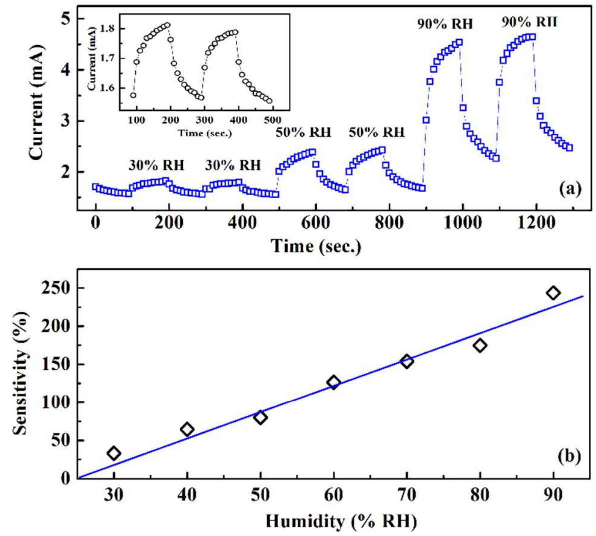

Fig. 8 (a) Dynamic responses of the n-MoS_2/p-Si junction upon consequent humidity at +4.0 V. The inset shows the enlarged image of the response to 30%RH. (b) Dependence of the sensing response of the junction on humidity levels.

Fig. 8(a) shows the dynamic response of the *n*-MoS_2/*p*-Si junction upon different humidity levels at +4.0 V, 30%RH, 50%RH and 90%RH, respectively. The inset shows the enlarged image of the response to 30%RH. From the figure, we can see that the junction shows significant response at each humidity level, even at 30%RH. When the conditions are changed alternately between dry air and humidity gas, two distinct current states for the junction are shown, the ‘‘low’’ current state in dry air and the ‘‘high’’ current state in humidity gas, respectively. Both the “high” and “low” states are stable and well reversible. The variation between two states is fast. Here, the response time (t_{res}) is defined as the time to rise from 10% to 90% of the total change and the recovery time (t_{rec}) is defined as the time to decay from 90% to 10% of the total change. According to the measured results, t_{res} and t_{rec} under the humidity level of 90%RH are about 36.3 s and 57.6 s, respectively. With decreasing the humidity levels, both t_{res} and t_{rec} increase continuously. Under 30%RH, t_{res} and t_{rec} are about 50.6 s and 63.8 s, respectively. As shown in the figure, the background current exhibits a positive slope over the total duration of the exposure due to the charge accumulation. From the figure, strong dependence of the response on humidity levels can be seen. Fig. 8(b) shows the dependence of the sensing response of the junction on humidity levels. As can be seen, an almost linear correlation is obtained in the measured range of humidity levels. When the junction is exposed to the humidity of 30%RH, *S* is about 33.7%. With increasing the humidity level, *S* increases gradually. When 90%RH, *S* reaches 243.7%.

RSC Advances

ARTICLE

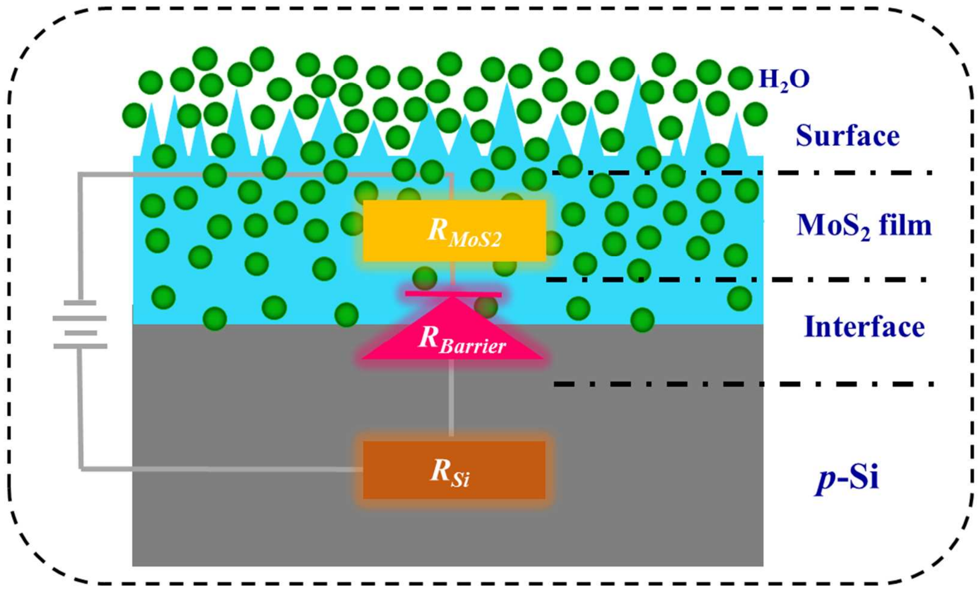

Fig. 9 Schematic of the n-MoS_2/p-Si junction under humidity condition and the equivalent circuit model of the heterojunction for current measurements.

According to theoretical calculations, H_2O molecules can be adsorbed on the surface of MoS_2 due to the charge transfer between them.[21] The interaction between the adsorbed gas molecules and underlying MoS_2 is physisorption because of the small adsorption energy and large separation distance.[22] Thus, fast response to humidity and recovery for MoS_2-based materials could be realized. As shown in Fig. 3, the surface of the as-grown MoS_2 film on Si is composed of cone-like grains. Large quantities of nanoscale grains could increase greatly the contact area of MoS_2 to H_2O molecules. Fig. 9(a) shows the schematic of the n-MoS_2/p-Si junction under ambient humidity conditions. When the n-MoS_2/p-Si junction is exposed to humidity gas, large numbers of H_2O molecules can be adsorbed on the surface of MoS_2 film. Subsequently, some of the adsorbed molecules could be capable of diffusing into the whole layer of the MoS_2 film through the pores caused by grain boundaries at the surface (shown in Fig.4), and even reach the interface area of the junction. As H_2O is an electron donor,[23] n-doping characteristics can be exhibited when H_2O molecules are adsorbed on the MoS_2 film. The Fermi level of the MoS_2 film is shifted towards the conduction band. Because of the n-type nature of the as-grown MoS_2 film, the carrier density of the film can be enhanced by the adsorbed H_2O molecules. On the other hand, the energy barrier (eV_{bi}) at MoS_2/Si interface increases due to the movement of the Fermi level of the film. Thus, the electrical transporting properties of the MoS_2/Si junction could be changed dramatically after H_2O adsorption. According to the equivalent circuit model of the heterojunction for current measurements in Fig. 9. The current through the sample is determined mainly by the resistance of the MoS_2 film (R_{MoS2}), the barrier resistance ($R_{Barrier}$) caused by the energy barrier at the interface and the resistance of the Si substrate (R_{Si}), $I=V/(R_{MoS2}+R_{Barrier}+R_{Si})$. During our experiments, R_{Si} is a constant and has not any change after the exposure to humidity condition. Thus, the response of the fabricated junction mainly originates from the effect of H_2O adsorption on R_{MoS2} and $R_{Barrier}$. Obviously, the adsorption has different effects on R_{MoS2} and $R_{Barrier}$. After adsorption, $R_{Barrier}$ increases due to the increase of the interfacial barrier height, while R_{MoS2} decreases due to the increase of the electron concentration in the film. When a forward voltage is applied on the sample, the junction is biased positively and the conduction of the sample is dominated by the film. Thus, the response of the heterojunction with the increase of the forward current can be seen from Fig. 7(a). With increasing the forward voltage, the interfacial barrier height decreases gradually. This weakens the effect of $R_{Barrier}$ on the conduction of the p-n junction. Thus, the sensitivity increases with increasing the forward voltage, as shown in Fig. 7(b). After a threshold voltage (+1.9 V), the interfacial barrier vanishes and the conduction of the p-n junction is controlled completely by the MoS_2 film. At this condition, the sensitivity becomes saturated and almost no change with further increasing the voltage, which is similar with that for the single MoS_2 sensor devices.[20] When a reverse voltage is applied, the junction is biased negatively and the interfacial barrier height increases. The charges near the interface are depleted and one depletion layer at the MoS_2/Si interface can be formed. At this condition, the external voltage almost drops on the depletion layer and the conduction is controlled by $R_{Barrier}$. Thus, the reverse current decreases when the dry-air conditions are changed into humidity conditions, as shown in Fig. 7. This is contrary to the current change in forward voltage range in the humidity condition. As shown in Fig. 4, the MoS_2 film deposited at RT has much smaller pore size than the film deposited at 400 °C. Comparatively, it is more difficult for H_2O molecules on the surface of the film deposited at RT to inject into the body. Thus, weak response to humidity gas can be seen in the junction with the MoS_2 film deposited at RT, while strong response can be exhibited in the junction with the film deposited at 400 °C.

When humidity conditions are changed into dry-air conditions, the adsorbed H_2O molecules are desorbed easily from the MoS_2 film due to their physisorption nature and small adsorption energies. As a result, the original electron concentration of MoS_2 films is recovered and so is the junction current. Thus, the *n*-MoS_2/*p*-Si junction exhibits humidity gas sensing properties, as shown in Fig. 8.

Conclusions

Bulk-like MoS_2 thin films were grown on *p*-type Si substrates by dc magnetron sputtering technique and *n*-MoS_2/*p*-Si junctions were fabricated. The fabricated junction exhibited obvious sensing properties to different humidity levels. In the forward voltage range, the currents increased significantly after the junction were exposed to humidity gas and the sensitivity increased with increasing voltage. The reverse current decreases under humidity conditions. An almost linear correlation was obtained in the measured range of humidity levels. This work demonstrates that *n*-MoS_2/*p*-Si junctions have a large potential application in the area of humidity sensing.

Acknowledgements

The authors would like to acknowledge the financial support by the Fundamental Research Funds for the Central Universities (14CX05038A), Fundamental Research Funds for the Central Universities (15CX08009A) and the National Science Foundation of China (Grant No.51502348, 51102284, 51372030 and 21476262).

References

1 B. Radisavljevic, A. Radenovi, J. Brivio, V. Giacometti and A. Kis, *Nat. Nanotechnol.*, 2011, **6**, 147; C. Ataca, H. Sahin, E. Aktuörk and S. Ciraci, *J. Phys. Chem. C*, 2011, **115**, 3934; M. Bernardi, M. Palummo and J. C. Grossman, *Nano Lett.*, 2013, **13**, 3664.
2 Y. Yoon, K. Ganapathi and S. Salahuddin, Nano Lett., 2011, 11, 3768; R. Ganatra and Q. Zhang, ACS Nano, 2014, 8, 4074.
3 K. Lee , R. Gatensby , N. McEvoy , T. Hallam and G. S. Duesberg, Adv. Mater., 2013, 25, 6699; Y. Yao, L. Tolentino, Z. Yang , X. Song, W. Zhang, Y. Chen and C. Wong, *Adv. Funct. Mater.*, 2013, **23**, 3577.
4 L. Hao, Y. Liu, W. Gao, Z. Han, Q. Xue, H. Zeng, Z. Wu, J. Zhu and W. Zhang, *J. Appl. Phys.*, 2015, **117**, 114502; S. Wi, H. Kim, M. Chen, H. Nam, L. J. Guo, E. Meyhofer and X. Liang, *ACS Nano*, 2014, **8**, 5270; K. Jiao, C. Duan, X. Wu, J. Chen, Y. Wang and Y. Chen, *Phys.Chem.Chem.Phys.*, 2015, **17**, 8182.
5 S. L. Zhang, H. H. Choi, H. Y. Yue and W. C. Yang, *Current Appl. Phys.*, 2014, **14**, 264.
6 X. Y. Feng, W. F. Chen and L. F. Yan, *Sensors and Actuators B: Chem.*, 2015, **215**, 316.
7 X. Gao, X. Zhang, C. Wan, X. Zhang, L. Wu and X. Tan, *Appl. Phys. Lett.*, 2010, **97**, 212101.
8 K. Jiang, T. Fei and T. Zhang, *RSC Adv.*, 2014, **4**, 28451.
9 H. Li, Z. Yin, Q. He, H. Li, X. Huang, G. Lu, D. Fam, A. Tok, Q. Zhang and H. Zhang, *Small*, 2012, **8**, 63; D. Sarkar, W. Liu, X. Xie, A. C. Anselmo, S. Mitragotri and K. Banerjee, *ACS Nano*, 2014, **8**, 3992; F. K. Perkins, A. L. Friedman, E. Cobas, P. M. Campbell, G. G. Jernigan and B. T. Jonker, *Nano Lett.*, 2013, **13**, 668.
10 L. Wang, J. Jie, Z. Shao, Q. Zhang, X. Zhang, Y. Wang, Z. Sun and S. T. Lee, *Adv. Func. Mater.*, 2015, **25**, 2910; M. R. Esmaeili-Rad and S. Salahuddin, *Sci. Rep.*, 2013, **3**, 2345.
11 Y. Liu, L. Hao, W. Gao, Z. Wu, Y. Lin, G. Li,W. Guo, L. Yu, H. Zeng, J. Zhu and W. Zhang, *Sensors and Actuators B: Chem.*, 2015, **211**, 537; Y. Liu, L. Hao, W. Gao, Q. Xue, W. Guo, Z. Wu, Y. Lin, H. Zeng, J. Zhu and W. Zhang, *J. All. Comp.*, 2015, **631**, 105.
12 D. R. Miller, S. A. Akbar and P. A. Morris, *Sensors and Actuators B: Chem.*, 2014, **204**, 250; S. Bai, D. Li, D. Han, R. Luo, A. Chena and C. L. Chung, *Sensors and Actuators B: Chem.*, 2010, **150**, 749; M. Ivanovskaya, D. Kotsikau, G. Faglia and P. Nelli, *Sensors and Actuators B: Chem.*, 2003, **96**, 498.
13 R. Ganatra and Q. Zhang, *ACS Nano*, 2014, **8**, 4074; Y. H. Lee, X. Q. Zhang, W. Zhang , M. T. Chang , C. T. Lin, K. D. Chang, Y. C. Yu, J. T. W. Wang, C. S. Chang, L. J. Li , and T. W. Lin, *Adv. Mater.*, 2012, **24**, 2320.
14 D. J. Late, P.A. Shaikh, R. Khare, R.V. Kashid, M. Chaudhary, M.A. More and S.B. Ogale, *ACS Appl. Mater. Interf.*, 2014, **6**, 15881.
15 H. Huang, G. Fang, X. Mo, L. Yuan, H. Zhou, M. Wang, H. Xiao and X. Zhao, *Appl. Phys. Lett.*, 2009, **94**, 063512.
16 L. Z. Hao, W. Gao, Y. J. Liu, Z. D. Han, Q. Z. Xue, W. Y. Guo, J. Zhu and Y. R. Li, *Nanoscale*, 2015, **7**, 8304.
17 S. M. Sze and K. K. Ng, *Physics of Semiconductor Devices, 3rd ed.*, Wiley, New York, 2007.
18 D. A. Neamen, *Semiconductor Physics and Devices: Basic Principles*, McGraw-Hill, New York, 2003.
19 M. Fontana, T. Deppe, A.K. Boyd, M. Rinzan, A.Y. Liu, M. Paranjape and P. Barbara, *Sci. Rep.*, 2013, **3**, 1634.
20 X. Wang, S. Yang, Q. Yue, F. Wu and J. Li, *J. All. Comp.*, 2014, **615**, 989.
21 Q. Yue, Z. Shao, S. Chang and J. Li, *Nano Research Lett.*, 2013, **8**, 425.
22 B. Cho, M. G. Hahm, M. Choi, J. Yoon, A. R. Kim, Y. J. Lee, S. G. Park, J. D. Kwon, C. S. Kim, M. Song, Y. Jeong, K. S. Nam, S. Lee, T. J. Yoo, C. G. Kang, B. H. Lee, H. C. Ko, P. M. Ajayan and D. H. Kim, *Sci. Rep.*, 2015, **5**, 8052.
23 D. J. Late, Y. K. Huang, B. Liu, J. Acharya, S. N. Shirodkar, J. Luo, A. Yan, D. Charles, U. V. Waghmare, V. P. Dravid and C. N. R. Rao, *ACS Nano*, 2013, **7**, 4879.

